Supramolecular nanostructures with tunable donor loading for controlled H$_2$S release

Yin Wang, **John B. Matson**[*]

Department of Chemistry, Virginia Tech Center for Drug Discovery, and Macromolecules Innovation Institute, Virginia Tech, Blacksburg, VA 24061, United States

Abstract

Hydrogen sulfide (H$_2$S), an endogenously generated and regulated signaling gas, plays a vital role in a variety of (patho)physiological processes. In the past few years, different kinds of H$_2$S-releasing compounds (often referred to as H$_2$S donors) have been developed for H$_2$S delivery, but it is still challenging to make H$_2$S donors with tunable payloads in a simple and efficient manner. Herein, a series of peptide-H$_2$S donor conjugates (PHDCs) with tunable donor loadings are designed for controlled H$_2$S release. The PHDCs self-assemble into nanoribbons with different geometries in aqueous solution. Upon addition of cysteine, these nanostructures release H$_2$S, delivering their payload into H9C2 cells, as visualized using an H$_2$S-selective fluorescent probe. Beyond imaging, *in vitro* studies show that the ability of PHDCs to mitigate doxorubicin-induced cardiotoxicity in H9C2 cardiomyocytes depends on their nanostructures and H$_2$S release profiles. This strategy may enable the development of sophisticated H$_2$S-releasing biomaterials for drug delivery and regenerative medicine.
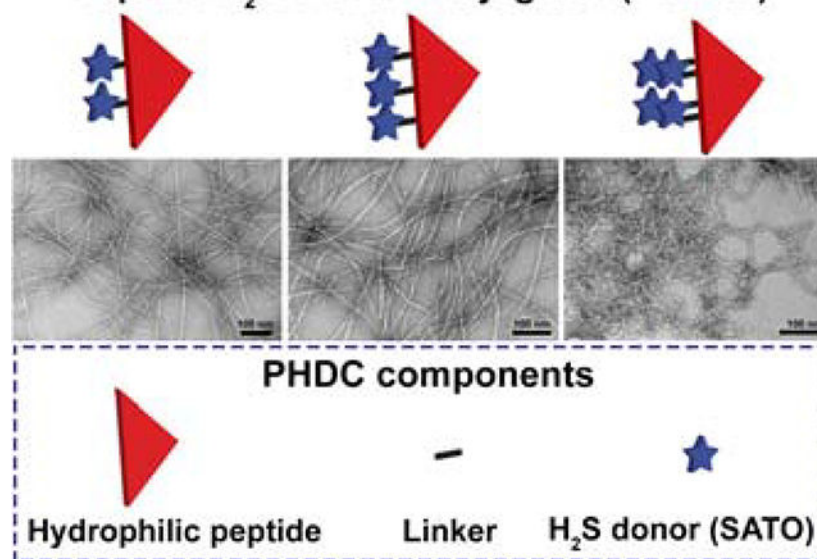
Graphical Abstract

[*]Corresponding Author jbmatson@vt.edu.

Payload Tunable Self-Assembling Peptide-H₂S Donor Conjugates (PHDCs)

PHDC components

Hydrophilic peptide   Linker   H₂S donor (SATO)

INTRODUCTION

As a biological signaling molecule, hydrogen sulfide (H_2S) is involved in many physiological and/or pathological processes such as vasodilation and angiogenesis.[1–4] Although the majority of foundational reports in this area used inorganic salts such as sodium sulfide (Na_2S) or sodium hydrosulfide (NaSH) as H_2S sources,[5–6] these molecules are not ideal compounds for studying H_2S biology due to their instantaneous release profiles and the transient nature of this signaling gas. In order to provide tools for studying H_2S biology with slow and sustained rates of H_2S delivery, several groups have recently developed many H_2S-releasing compounds (so-called H_2S donors).[7–12] These donors respond to specific triggers, releasing H_2S after application of a stimulus such as light, biologically-relevant thiols, changes in pH, enzymatic activity, and many others. However, despite this variety of synthetic H_2S donors, several issues still need to be addressed. Low water solubility, few methods to tune release kinetics, and in most cases no capacity for delivery to a specific biological target limit the use of many H_2S donors both as chemical tools for investigating the biological roles of H_2S and as potential therapeutics.

One promising strategy to address these limitations is to incorporate H_2S donors into materials, either through physical encapsulation[13–14] or by covalent conjugation to hydrophilic polymers.[15–18] While these methods can be effective, the short- and long-term biological activities, combined with potential toxicity arising from the synthetic polymers, may be cause for concern.[19] Additionally, polydispersity must be considered, referring here both to polymer length and the amount of conjugated H_2S donor, making polymeric drug

delivery vehicles of all kinds consistently vulnerable to batch-to-batch variability. To circumvent these problems, we began designing and evaluating H_2S-releasing materials based on self-assembling peptides.[20–24] Peptides are useful materials from which to build self-assembled nanostructures for biomedical applications due to their inherent biodegradability and biocompatibility under many circumstances.[25] Moreover, they can be quickly synthesized and purified with direct sequence control.[26–27] Previously, our group showed that H_2S-donating S-aroylthiooximes (SATOs) appended to the hexapeptide Ile-Ala-Val-Glu-Glu-Glu (IAVEEE) assembled into nanofibers in water.[20] The nanostructures protected the SATO groups from hydrolytic decomposition and prolonged the release time in water as compared to small molecule SATOs. Very recently, we found that conjugation of SATOs to short tetrapeptides not only extended their H_2S release profiles, but also modulated their release behaviors as a result of their different self-assembled morphologies.[21]

Despite progress in developing peptide-based H_2S donors, a remaining downside of existing constructs is their limited tunability in terms of donor loading. A series of H_2S-donating peptides with variable numbers of SATO groups per peptide has not been explored. In this context, we report here a group of peptide-H_2S donor conjugates (PHDCs) that self-assemble in water to form stable supramolecular nanostructures with an ability to tune the SATO loading by molecular design. We aimed to evaluate how donor loading affects the self-assembled morphology, H_2S release profiles, and biological activity of these PHDCs.

To achieve this goal, we appended SATOs, a thiol-triggered H_2S donor developed in our lab,[28] onto peptide sequences of 2–7 amino acids. Specifically, S-benzoylthiohydroxylamine (SBTHA) was added to three peptides, each with the same pentapeptide, Phe-Glu-Glu-Glu-Glu (FE_4), but with different numbers of 4-formylbenzoic acid (FBA) units attached to Lys residues on the side chain ε-amine or the N-terminus. This molecular design allowed us to precisely attach two, three, or four SATOs onto the peptides, corresponding to respective SATO loadings of 24%, 28% and 31% by weight (Eq. S1–3). The structures of these three PHDCs are shown in Figure 1 and are labeled **dSATO-FE₄**, **tSATO-FE₄**, and **qSATO-FE₄** for short. Synthetic procedures and characterization details are included in the Supporting Information (Figure S1).

RESULTS AND DISCUSSION

We first probed each PHDC after dissolution in aqueous 10 mM phosphate buffer (pH 7.4) by conventional transmission electron microscopy (TEM). Images showed that all three PHDCs assembled into long, one-dimensional nanostructures (Figure 1D–F). The dominant morphology observed for PHDC **dSATO-FE₄** was twisted ribbons (Figure 1D). The widths were 7±1 nm, and average lengths were a few micrometers. PHDC **tSATO-FE₄** also formed twisted ribbons 7±1 nm in width and several micrometers in length (Figure 1E). In contrast, a different morphology was observed for PHDC **qSATO-FE₄**. It associated into curved ribbons with average widths of 6±1 nm (Figure 1F). Although not as long as the twisted ribbons formed by **dSATO-FE₄** and **tSATO-FE₄**, the curved ribbons tended to form bundles, which we expected could be beneficial for prolonging H_2S release. These results

show how incorporating different numbers of SATOs into the PHDC structure allows for tuning of both the SATO loading content and the self-assembled morphologies.

To probe the differences among these PHDCs in their self-assembled states, we began by conducting Nile Red assays to measure their critical aggregation concentrations (CACs), followed by circular dichroism (CD) spectroscopy to study the secondary structures of the self-assembled PHDCs. The Nile Red assay showed that the CAC value for each of the three PHDCs was between 20 and 30 μM (Figure S2 and Table S1). This is consistent with previous CAC measurements on PHDCs.[21] Despite their similar self-assembled morphologies, CD spectroscopy revealed that the secondary structures of these PHDC nanostructures were quite different. All three exhibited signals in the peptide region (190–240 nm), where amide bonds in peptides absorb, and in the SATO region (300–360 nm). Absorptions in the SATO region are consistent with UV-vis absorption peaks (Figure S3). In the peptide region, the spectra for both **dSATO-FE$_4$** (Figure 2A) and **qSATO-FE$_4$** (Figure 2C) showed primarily random coil structure with some amount of α-helix, although the intensity in the peptide region for **qSATO-FE$_4$** was substantially greater than that for **dSATO-FE$_4$**. In contrast, the CD spectrum for **tSATO-FE$_4$** was consistent with both a β-sheet structure, as indicated by the positive peak at 215 nm, and some random coil contribution (Figure 2B). These data indicate that secondary structures of these nanoassemblies are quite sensitive to the nature of the hydrophobic component, even though the peptide sequences are similar. The absorption of each PHDC varied in the SATO region as well. PHDCs **dSATO-FE$_4$** and **qSATO-FE$_4$** showed negative peaks near 330 nm, with **qSATO-FE$_4$** exhibiting a much more intense peak than **dSATO-FE$_4$**. Unlike the negative absorption peaks of **dSATO-FE$_4$** and **qSATO-FE$_4$** in the SATO region, **tSATO-FE$_4$** exhibited a positive peak in the same range, possibly due to different handedness within these nanoribbons.[29] The intensity of the SATO peak for **tSATO-FE$_4$** was between that of **dSATO-FE$_4$** and **qSATO-FE$_4$**. We speculate that the observed intensity differences in this region among the three PHDCs is a result of increased hydrophobic effects and therefore stronger molecular packing among SATO groups as more SATO groups are introduced into the molecular design.

We next examined how the H$_2$S release profiles of the three PHDCs was affected by their supramolecular structure. Because these PHDCs self-assemble in water, we expected that the nanostructures would shield SATO components from the aqueous environment, providing a method to control release of H$_2$S triggered by cysteine (Cys). We typically assess release profiles from H$_2$S donors by an H$_2$S-selective microelectrode probe. This method provides a real-time measurement of H$_2$S solution concentration; however, it is not capable of providing cumulative release curves because H$_2$S volatilizes and oxidizes as it is produced. Therefore, H$_2$S release profiles obtained with this electrochemical probe-based method are often compared using peaking times, which provide an approximate quantification of relative release rates among similar samples.

H$_2$S release from these PHDCs was triggered by Cys, which we and others use commonly to trigger release of H$_2$S from SATO-based materials.[16, 20–21, 30] In order to eliminate the false response from the electrochemical probe generated by Cys, we used a specially made vial, reported previously,[21] to evaluate PHDC release profiles. In these experiments, the releasing

solution was loaded into the inner well of the vial; next the well was sealed with a gas-permeable membrane (Figure S4). We kept PHDC concentration in the inner well at 1 mM while varying the amounts of Cys (4 mM total Cys for **dSATO-FE₄**, 6 mM for **tSATO-FE₄**, and 8 mM for **qSATO-FE₄**) to keep the molar ratio of SATO to Cys at 1:2. The concentration of H_2S as it passed from the inner well into a large volume of PBS was then monitored over time.

All three PHDCs showed steady and consistent H_2S release lasting for several hours (Figure 3A). Although all three PHDCs formed nanoribbons, the H_2S release profiles were quite different. Both **dSATO-FE₄** and **tSATO-FE₄** released H_2S immediately after addition of Cys. Compared with the steady release profile of **dSATO-FE₄**, there was a plateau for **tSATO-FE₄** after 20 min, and then the release rate accelerated. This interesting release profile may result from a morphology change during the H_2S release process. With three SATOs toward the N-terminal end of the peptide, Cys penetration into the core of the assemblies would not lead to reaction of all three SATOs at the same time, leading to a decrease in the magnitude of the hydrophobic and π–π interactions, changing the morphology. These newly formed nanostructures would therefore be expected to release H_2S faster as the packing among SATOs becomes weaker and the nanostructures loosen. Therefore, the observed release profile would be a combination from different nanostructures. Despite the different profiles, peaking times for **dSATO-FE₄** and **tSATO-FE₄** were quite similar, at 127±8 and 136±7 min, while the peaking time for **qSATO-FE₄** was significantly longer at 181±4 min (Figure 3B). Interestingly, unlike the profiles for **dSATO-FE₄** and **tSATO-FE₄**, we observed an induction period of 50 min for **qSATO-FE₄** where H_2S was slowly released, after which the rate of release increased sharply. This induction time phenomenon was also observed in a different PHDC system reported by our group recently.[21] We speculate that this initial period of slow release from **qSATO-FE₄** results from Cys diffusing more slowly into the short, curved nanoribbon bundles formed by **qSATO-FE₄** (Figure 1F) compared with the separated nanoribbons in the other two PHDCs. In order to investigate the concentration effect on H_2S release, we performed H_2S release experiments with PHDC concentrations of 100 μM in the inner well were carried out. As shown in Figure S5 and Table S2, shorter peaking times were observed at 100 μM than at 1 mM despite the 10-fold dilution. Additionally, no significant difference in peaking times was observed, and no induction time was noted for any of the three PHDCs. These results resemble those from other drug-releasing self-assembling peptides[31–32] and our recently reported PHDC tetrapeptides,[21] where the release rate increases upon dilution of the samples. These data collectively indicate that Cys penetrated into these nanoribbons in a similar manner regardless of the varying number of SATO groups when the concentration of PHDC was low, but that rates of Cys diffusion varied at higher PHDC concentrations.

We then turned our attention to biological studies on PHDCs **dSATO-FE₄** and **qSATO-FE₄**, which had the shortest and longest peaking times. Fluorescence microscopy was used to investigate whether **dSATO-FE₄** and **qSATO-FE₄** could be deliver H_2S into cells. We used WSP-5,[33] an H_2S-selective fluorescent probe, to monitor H_2S accumulation from these PHDCs in H9C2 cells. As expected, Cys alone provided no fluorescent signal, because WSP-5 responds to H_2S but not to Cys (Figure 4, first row).[33] Treating cells with PHDCs

without Cys provided a weak fluorescent signal, which likely resulted from a small amount of H_2S generated from hydrolysis of PHDCs (Figure 4, second and third rows). In sharp contrast, co-addition of **dSATO-FE$_4$** or **qSATO-FE$_4$** with Cys resulted in a significant increase in WSP-5 fluorescence (Figure 4, fourth and fifth rows), demonstrating that both **dSATO-FE$_4$** and **qSATO-FE$_4$** can be successfully activated to release H_2S *in vitro* and that the released H_2S can be imaged using an H_2S-responsive fluorescent probe.

Given that both PHDCs were capable of delivering H_2S into cells, we next explored their ability to protect against cardiotoxicity induced by doxorubicin (Dox), a common chemotherapeutic. Dox, an anthracycline with widespread antitumor activity, has potent therapeutic effects on a variety of cancers, including lymphomas, leukemias, soft-tissue sarcomas, and various types of solid tumors.[34] However, its clinical use is limited by its dose-limiting and at times life-threatening cardiotoxicity.[35] Previous studies showed that H_2S, delivered as instantaneously releasing Na_2S, rescues cardiomyocytes treated with Dox by mitigating stress in the endoplasmic reticulum,[36–37] or depressing the p38 MAPK pathway,[38–39] but this cardioprotective capacity has not been tested widely on sustaained H_2S donors.[21] More importantly, slow-releasing H_2S donors frequently lead to enhanced biological effects compared to instantaneously releasing Na_2S.[16, 40] Thus, we envisioned that the PHDCs developed here might rescue cardiomyocytes in the presence of Cys.

First, we confirmed that both **dSATO-FE$_4$** at 200 μM and **qSATO-FE$_4$** at 100 μM (both 400 μM SATO) were nontoxic to H9C2 cells in the presence of Cys (left two columns in Figure 5). In treatment studies, H9C2 cells were pretreated with **dSATO-FE$_4$** and **qSATO-FE$_4$** in the presence of Cys for 30 min.[21, 36, 41] Without removing the PHDC/Cys solution, Dox was added and cells were incubated for another 24 h. Compared to the Dox only treatment group (46% viability, brown column in Figure 5), cell viability increased significantly when cells were treated with **dSATO-FE$_4$** (69% viability) or **qSATO-FE$_4$** (84% viability) (black and blue columns on the right in Figure 5). More importantly, **qSATO-FE$_4$** was significantly more effective in rescuing cells than **dSATO-FE$_4$**. Because PHDCs were added in amounts to keep SATO loadings equal, this difference in bioactivity is likely due to the following two phenomena: 1) PHDC stock solutions (2 mM **dSATO-FE$_4$** and 4 mM **qSATO-FE$_4$**) were added to cell media immediately before adding media to the cells, preserving their original morphologies; 2) The length of **qSATO-FE$_4$** curved ribbons are much shorter than that the **dSATO-FE$_4$** nanoribbons (Figure 1), which may facilitate cell uptake. Finally, we also confirmed that sustained H_2S release was key for rescuing cardiomyocytes treated with Dox through comparisons to other H_2S donors and control compounds (Figure S6), including Cys alone (49% viability), GYY4137 (38% viability), and Na_2S (56% viability). Taken together, these results highlight the importance of release rate on H_2S bioactivity.

CONCLUSIONS

In summary, we discuss here the synthesis and self-assembly of discrete PHDC nanostructures with tunable H_2S donor content by controlling the number of H_2S-releasing SATO units near the peptide N-terminus. The release behaviors depended strongly on the self-assembled morphology of the PHDCs, which relied heavily on molecular design, with the peaking time prolonged as the SATO loading percentage increased. *In vitro* fluorescence

studies showed that in the presence of Cys, H$_2$S released from PHDCs could be delivered into cells and visualized using an H$_2$S-responsive fluorescent probe. In addition, the released H$_2$S mitigated Dox-induced toxicity in H9C2 cardiomyoctyes, in which the PHDC with more SATO loading was more effective than its counterparts. These results highlight how variation in payload loading in amphiphilic peptides not only regulates the resulting self-assembled morphology, but also can modulate the bioactivity of these molecules. As the number of bioactive or drug molecules on a peptide can be easily changed by tuning the molecular design, we believe this strategy offers a general method to fabricate multiple types of nanostructures carrying a particular payload, enabling nanostructure-activity studies, such as this one, to be conducted on a wide variety of systems.

Supplementary Material

Refer to Web version on PubMed Central for supplementary material.

ACKNOWLEDGMENT

REFERENCES

(1). Wang R, Physiological implications of hydrogen sulfide: a whiff exploration that blossomed. Physiol. Rev. 2012, 92, 791–896. [PubMed: 22535897]

(2). Szabo C, Gasotransmitters in cancer: from pathophysiology to experimental therapy. Nat. Rev. Drug Discov. 2016, 15, 185–203. [PubMed: 26678620]

(3). King AL; Polhemus DJ; Bhushan S; Otsuka H; Kondo K; Nicholson CK; Bradley JM; Islam KN; Calvert JW; Tao YX; Dugas TR; Kelley EE; Elrod JW; Huang PL; Wang R; Lefer DJ, Hydrogen sulfide cytoprotective signaling is endothelial nitric oxide synthase-nitric oxide dependent. Proc. Natl. Acad. Sci. U. S. A. 2014, 111, 3182–3187. [PubMed: 24516168]

(4). Kimura H, Production and physiological effects of hydrogen sulfide. Antioxid. Redox Signal. 2014, 20, 783–793. [PubMed: 23581969]

(5). Zhao WM; Zhang J; Lu YJ; Wang R, The vasorelaxant effect of H$_2$S as a novel endogenous gaseous K-ATP channel opener. Embo J. 2001, 20, 6008–6016. [PubMed: 11689441]

(6). Jha S; Calvert JW; Duranski MR; Ramachandran A; Lefer DJ, Hydrogen sulfide attenuates hepatic ischemia-reperfusion injury: role of antioxidant and antiapoptotic signaling. Am. J. Physiol.-Heart Circul. Physiol. 2008, 295, H801–H806.

(7). Hartle MD; Pluth MD, A practical guide to working with H$_2$S at the interface of chemistry and biology. Chem. Soc. Rev. 2016, 45, 6108–6117. [PubMed: 27167579]

(8). Powell CR; Dillon KM; Matson JB, A review of hydrogen sulfide (H2S) donors: chemistry and potential therapeutic applications. Biochem. Pharmacol. 2018, 149, 110–123. [PubMed: 29175421]

(9). Zhao Y; Biggs TD; Xian M, Hydrogen sulfide (H2S) releasing agents: chemistry and biological applications. Chem. Comm. 2014, 50, 11788–11805. [PubMed: 25019301]

(10). Zhao Y; Henthorn HA; Pluth MD, Kinetic insights into hydrogen sulfide delivery from caged-carbonyl sulfide isomeric donor platforms. J. Am. Chem. Soc. 2017, 139, 16365–16376. [PubMed: 29056039]

(11). Chauhan P; Bora P; Ravikumar G; Jos S; Chakrapani H, Esterase activated carbonyl sulfide/hydrogen sulfide (H2S) donors. Org. Lett. 2017, 19, 62–65. [PubMed: 27996277]

(12). Zhao Y; Wang H; Xian M, Cysteine-activated hydrogen sulfide (H2S) donors. J. Am. Chem. Soc. 2011, 133, 15–17. [PubMed: 21142018]

(13). Feng S; Zhao Y; Xian M; Wang Q, Biological thiols-triggered hydrogen sulfide releasing microfibers for tissue engineering applications. Acta Biomater. 2015, 27, 205–213. [PubMed: 26363376]

(14). Connal LA, The benefits of macromolecular hydrogen sulfide prodrugs. J. Mater. Chem. B 2018, 6, 7122–7128. [PubMed: 32254628]

(15). Urquhart MC; Ercole F; Whittaker MR; Boyd BJ; Davis TP; Quinn JF, Recent advances in the delivery of hydrogen sulfide via a macromolecular approach. Polym. Chem. 2018, 9, 4431–4439.

(16). Foster JC; Radzinski SC; Zou XL; Finkielstein CV; Matson JB, H2S-releasing polymer micelles for studying selective cell toxicity. Mol. Pharm. 2017, 14, 1300–1306. [PubMed: 28300411]

(17). Hasegawa U; van der Vlies AJ, Design and synthesis of polymeric hydrogen sulfide donors. Bioconjugate Chem. 2014, 25, 1290–1300.

(18). Takatani-Nakase T; Katayama M; Matsui C; Hanaoka K; van der Vlies AJ; Takahashi K; Nakase I; Hasegawa U, Hydrogen sulfide donor micelles protect cardiomyocytes from ischemic cell death. Mol. Biosyst. 2017, 13, 1705–1708. [PubMed: 28681875]

(19). Dobrovolskaia MA; Mcneil SE, Immunological properties of engineered nanomaterials. Nat. Nanotechnol. 2007, 2, 469–478. [PubMed: 18654343]

(20). Carter JM; Qian Y; Foster JC; Matson JB, Peptide-based hydrogen sulphide-releasing gels. Chem. Commun. 2015, 51, 13131–13134.

(21). Wang Y; Kaur K; Scannelli SJ; Bitton R; Matson JB, Self-assembled nanostructures regulate H2S release from constitutionally isomeric peptides. J. Am. Chem. Soc. 2018, 140, 14945–14951. [PubMed: 30369241]

(22). Kaur K; Qian Y; Gandour RD; Matson JB, Hydrolytic decomposition of S-aroylthiooximes: effect of pH and N-arylidene substitution on reaction rate. J. Org. Chem. 2018, 83, 13363–13369. [PubMed: 30347157]

(23). Qian Y; Kaur K; Foster JC; Matson JB, Supramolecular tuning of H2S release from aromatic peptide amphiphile gels: effect of core unit substituents. Biomacromolecules 2019, 20, 1077–1086. [PubMed: 30676716]

(24). Longchamp A; Kaur K; Macabrey D; Dubuis C; Corpataux J-M; Déglise S; Matson JB; Allagnat F, Hydrogen sulfide-releasing peptide hydrogel limits the development of intimal hyperplasia in human vein segments. Acta Biomater. 2019, DOI: 10.1016/j.actbio.2019.07.042.

(25). Matson JB; Stupp SI, Self-assembling peptide scaffolds for regenerative medicine. Chem. Commun. 2012, 48, 26–33.

(26). Wang Y; Cheetham AG; Angacian G; Su H; Xie LS; Cui HG, Peptide-drug conjugates as effective prodrug strategies for targeted delivery. Adv. Drug Deliv. Rev. 2017, 110, 112–126. [PubMed: 27370248]

(27). Cui HG; Webber MJ; Stupp SI, Self-assembly of peptide amphiphiles: from molecules to nanostructures to biomaterials. Biopolymers 2010, 94, 1–18. [PubMed: 20091874]

(28). Foster JC; Powell CR; Radzinski SC; Matson JB, S-aroylthiooximes: a facile route to hydrogen sulfide releasing compounds with structure-dependent release kinetics. Org. Lett. 2014, 16, 1558–1561. [PubMed: 24575729]

(29). Xing Q; Zhang J; Xie Y; Wang Y; Qi W; Rao H; Su R; He Z, Aromatic motifs dictate nanohelix handedness of tripeptides. ACS Nano 2018, 12, 12305–12314. [PubMed: 30452865]

(30). Lin LH; Qin HR; Huang JB; Liang H; Quan DP; Lu J, Design and synthesis of an AIE-active polymeric H2S-donor with capacity for self-tracking. Polym. Chem 2018, 9, 2942–2950.

(31). Cheetham AG; Zhang PC; Lin YA; Lock LL; Cui HG, Supramolecular nanostructures formed by anticancer drug assembly. J. Am. Chem. Soc. 2013, 135, 2907–2910. [PubMed: 23379791]

(32). Lin R; Cheetham AG; Zhang PC; Lin YA; Cui HG, Supramolecular filaments containing a fixed 41% paclitaxel loading. Chem. Commun. 2013, 49, 4968–4970.

(33). Peng B; Chen W; Liu CR; Rosser EW; Pacheco A; Zhao Y; Aguilar HC; Xian M, Fluorescent probes based on nucleophilic substitution-cyclization for hydrogen sulfide detection and bioimaging. Chem.-Eur. J 2014, 20, 1010–1016. [PubMed: 24339269]

(34). Muggia FM; Green MD, New anthracycline antitumor antibiotics. Crit. Rev. Oncol. Hematol. 1991, 11, 43–64. [PubMed: 1831987]

(35). Scully RE; Lipshultz SE, Anthracycline cardiotoxicity in long-term survivors of childhood cancer. Cardiovas. Toxicol. 2007, 7, 122–128.

(36). Wang XY; Yang CT; Zheng DD; Mo LQ; Lan AP; Yang ZL; Hu F; Chen PX; Liao XX; Feng JQ, Hydrogen sulfide protects H9c2 cells against doxorubicin-induced cardiotoxicity through inhibition of endoplasmic reticulum stress. Mol. Cell. Biochem. 2012, 363, 419–426. [PubMed: 22203419]

(37). Chegaev K; Rolando B; Cortese D; Gazzano E; Buondonno I; Lazzarato L; Fanelli M; Hattinger CM; Serra M; Riganti C; Fruttero R; Ghigo D; Gasco A, H$_2$S-donating doxorubicins may overcome cardiotoxicity and multidrug resistance. J Med Chem 2016, 59, 4881–4889. [PubMed: 27120394]

(38). Guo RM; Lin JC; Xu WM; Shen N; Mo LQ; Zhang CR; Feng JQ, Hydrogen sulfide attenuates doxorubicin-induced cardiotoxicity by inhibition of the p38 MAPK pathway in H9c2 cells. Int. J. Mol. Med. 2013, 31, 644–650. [PubMed: 23338126]

(39). Guo R; Wu K; Chen J; Mo L; Hua X; Zheng D; Chen P; Chen G; Xu W; Feng J, Exogenous hydrogen sulfide protects against doxorubicin-induced inflammation and cytotoxicity by inhibiting p38MAPK/NFkB pathway in H9c2 cardiac cells. Cell. Physiol. Biochem. 2013, 32, 1668–1680. [PubMed: 24356372]

(40). Kang J; Li Z; Organ CL; Park C-M; Yang C.-t.; Pacheco A; Wang D; Lefer DJ; Xian M, pH-controlled hydrogen sulfide release for myocardial ischemia-reperfusion injury. J. Am. Chem. Soc. 2016, 138, 6336–6339. [PubMed: 27172143]

(41). Chen Y; Sun L; Wang Y; Zhao X, A dual-fluorescent whole-well imaging approach for screening active compounds against doxorubicin-induced cardiotoxicity from natural products. RSC Adv 2015, 5, 106431–106438.
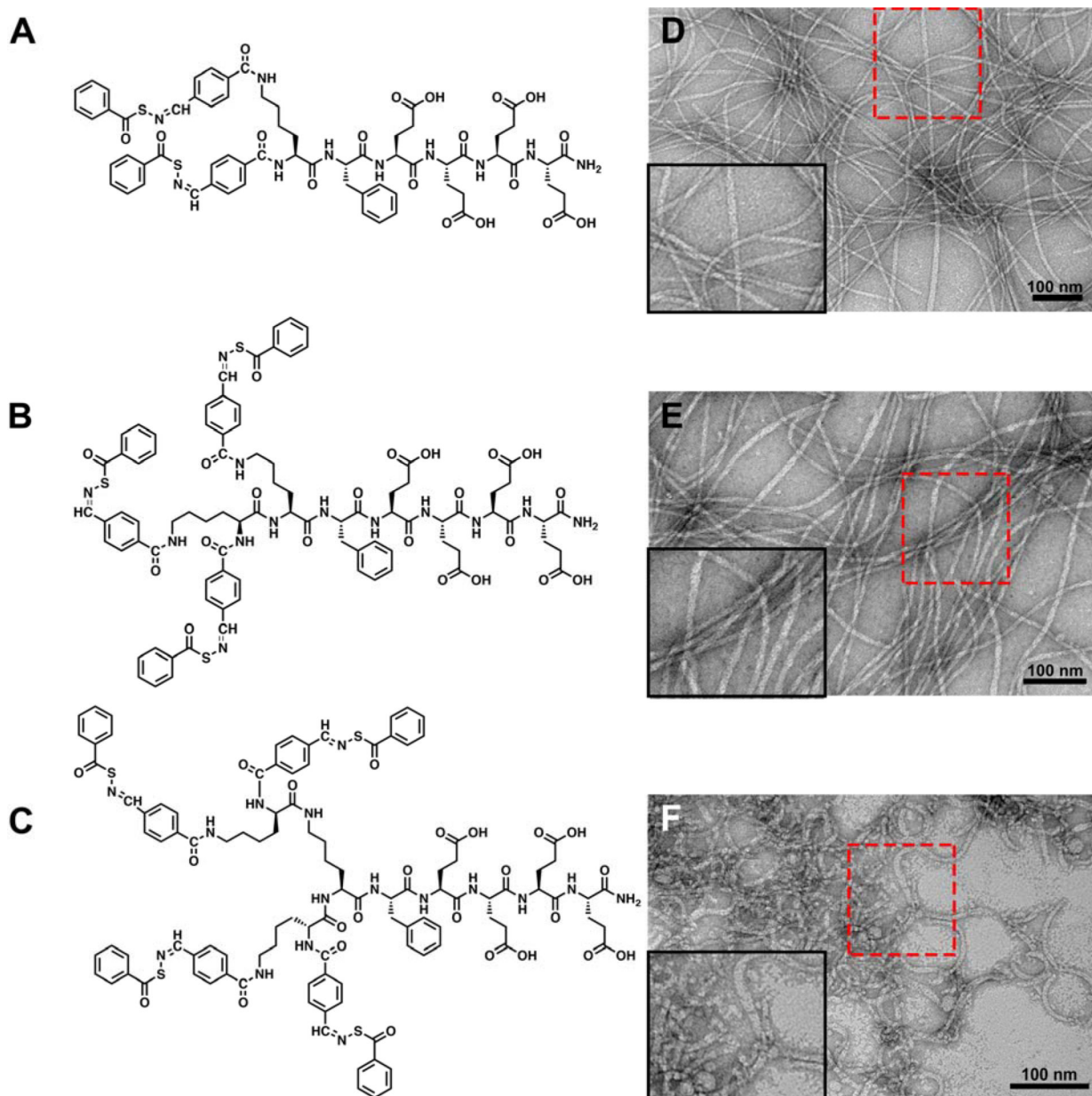
Figure 1.

(A-C) Molecular structures of PHDCs studied in the present work. (A) **dSATO-FE₄**; (B) **tSATO-FE₄**; (C) **qSATO-FE₄**. (D-F) Conventional TEM images illustrate the effect of SATO numbers on the self-assembled morphologies of the PHDCs in phosphate buffer (10 mM, pH 7.4). (D) Twisted ribbons formed by **dSATO-KFE₄**; (E) Twisted ribbons formed by **tSATO-FE₄**; (F) Curved ribbons formed by **qSATO-FE₄**. Inserts in the bottom left corners of panels D-F show zoomed-in images of the areas outlined by the red rectangles. Solution concentration: 100 μM peptides in phosphate buffer (pH 7.4). Uranyl acetate (UA) was used to stain all grids prior to imaging.
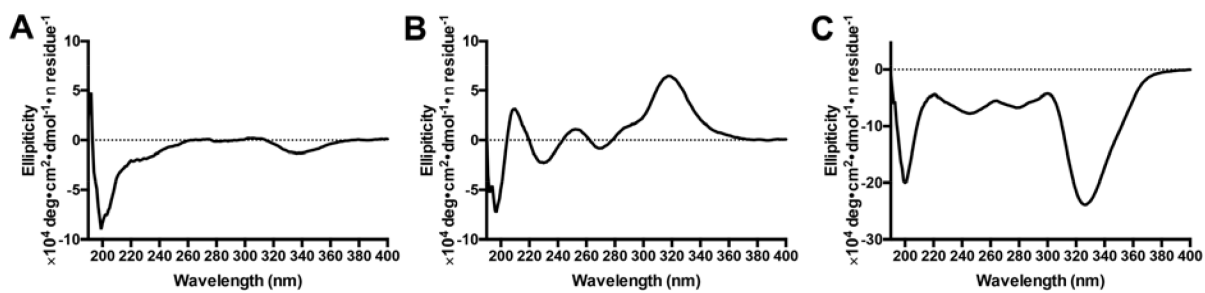
Figure 2.
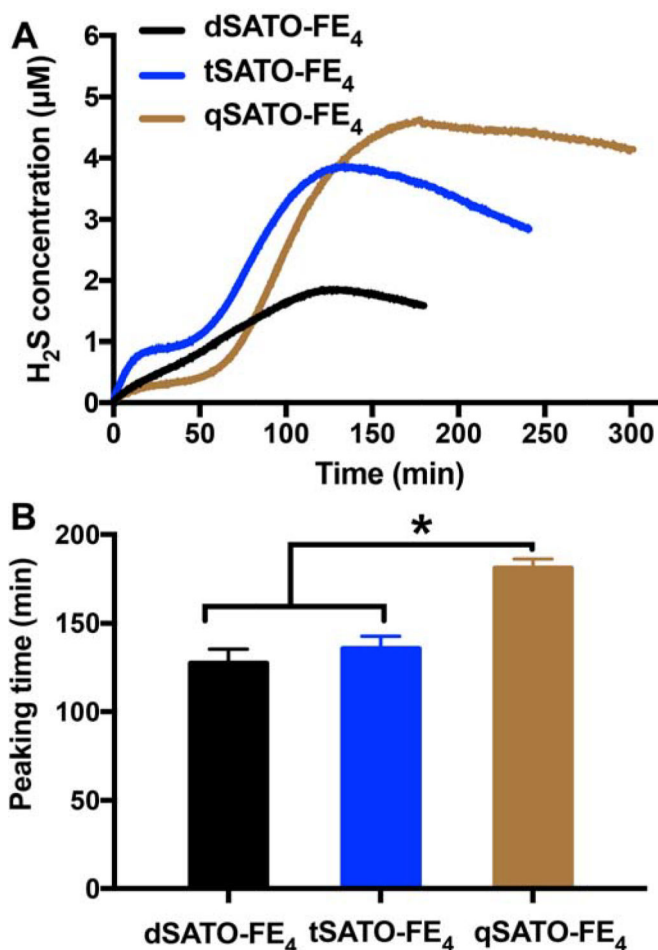CD spectra of (A) **dSATO-FE$_4$**, (B) **tSATO-FE$_4$**, and (C) **qSATO-FE$_4$** in phosphate buffer (75 μM, pH 7.4).

Figure 3.
(A) H$_2$S release profiles and (B) corresponding peaking times of **dSATO-FE$_4$**, **tSATO-FE$_4$**, and **qSATO-FE$_4$** triggered by Cys at rt in PBS (pH = 7.4). Data were obtained on an H$_2$S-sensitive electrochemical probe from a solution of PHDC (1 mM, 110 μL total) and Cys (4 mM for **dSATO-FE$_4$**, 6 mM for **tSATO-FE$_4$**, 8 mM for **qSATO-FE$_4$**) sealed in an inner well with a gas-permeable membrane inside a vial containing PBS (5 mL). Error bars indicate standard deviations of three separate experiments. * indicates p<0.05 for a comparison of the groups indicated as determined by a one-way analysis of variance (ANOVA) with a Student-Newman-Keuls comparisons *post-hoc* test (n=3).
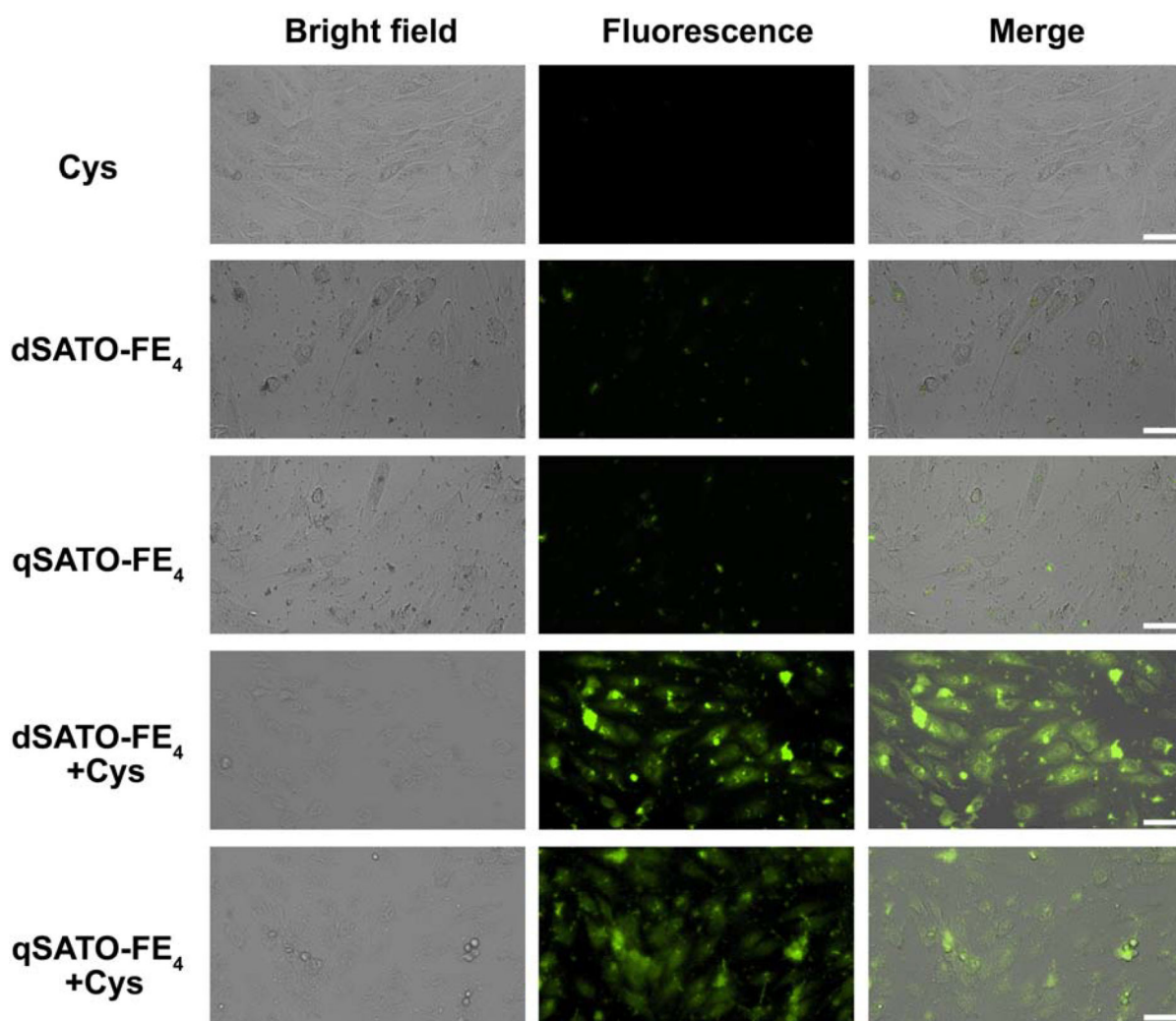
Figure 4.
Bright field, fluorescence, and merged images showing fluorescence in H9C2 cells pre-incubated with H$_2$S probe WSP-5 (50 μM) for 30 min and then treated with the following groups: Cys (800 μM), PHDC (200 μM for **dSATO-FE$_4$**; 100 μM for **qSATO-FE$_4$**) or PHDC and Cys for 2 h. Cells were then washed, and fluorescence images were taken in PBS. Scale bars are 50 μm.
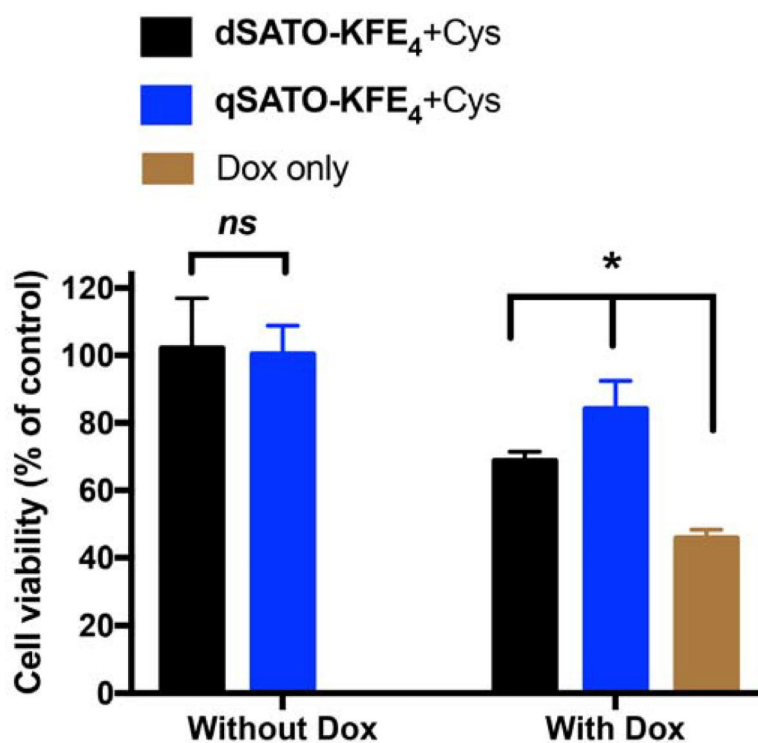
Figure 5.
Cell viability of H9C2 cardiomyoctyes pretreated with **dSATO-FE₄** (200 μM) or **qSATO-FE₄** (100 μM) in the presence of Cys (800 μM) for 30 min before Dox addition (5 μM) or not (control). * indicates p<0.01. Error bars indicate standard deviations of three separate experiments with five replicates per experiment. Group comparisons are indicated as determined by a one-way ANOVA with a Student-Newman-Keuls comparisons *post-hoc* test.